COMMUNICATION

Organic Base Modulation Triodes and Their Inverters on Flexible Substrates

By *Shiau-Shin Cheng, You-Che Chuang, Dhananjay Kekuda, Chun-Wei Ou, Meng-Chyi Wu,* and *Chi-Wei Chu**

Organic thin-film transistors (OTFTs), with the viewpoints of low cost/low temperature processing, mechanical flexibility, and large area coverage, have spurred tremendous interest within the development of consumable electronics and optoelectronics such as flat-panel display drivers, radio-frequency identification tags, smart cards, and sensors.[1–5] The typical architecture of OTFTs has adopted inorganic metal-oxide-semiconductor field-effect transistors in which the source and drain lie on the same plane above or below the semiconductor layer. Therefore, the performance of conventional TFTs is determined by two design parameters, the channel length (L) and field-effect mobility (μ_{FE}), in accordance with $t_{SD} = L^2/(\mu_{FE} \times V_{DD})$, where t_{SD} is the source–drain response time and V_{DD} the supply voltage.[6] Although, substantial progress has been achieved in developing new organic materials with higher μ_{FE}, typically confined to 1 $cm^2 V^{-1} s^{-1}$,[7] for conventional OTFTs, they still meet the lower operation frequencies and the higher operation voltages for some applications, which are mainly due to the low carrier mobility of organic semiconductors, and their frequency responses were also determined by the capacitance of the gate dielectric used. The design of TFTs with high performance relies mainly on the channel dimensions, for example the channel length. Hence, varying the channel length is a critical parameter in enhancing the carrier-transport properties across the drain/source in planar-type TFTs. However, shortening the channel length suffers from the incapability of integrating organic devices into nanolithographic techniques. Moreover, the contact resistance of semiconductors/metals limits the performance of devices while shortening the channel length down to sub-micrometer scales.[8]

An alternative approach to shorten the channel length is to adopt a vertical structure for transistors.[9–12] Since the conductive channel is in a perpendicular direction to the substrate, the channel length can be precisely controlled by organic-film thickness down to the micrometer or sub-micrometer regimes. Owing to this advantage of the short channel length, the operation frequency and the operation voltage can be dramatically improved, even when we use the existing organic semiconductors as channel materials. Accordingly, extensive progress has been achieved in the production of high-performance organic vertical-type transistors (OVTs) such as polymer grid triodes,[13] hot carrier transistors,[14,15] gate–source–drain transistors,[16,17] and metal-based organic transistors.[18] Although these OVTs present high device performances as compared to the conventional OTFTs, they still lack apparent saturation regions, which limit their use in low-power and high-frequency electronic applications.

In this communication, we demonstrate a promising vertical-type transistor, organic base modulation triode (OBMT), which is fabricated employing two back-to-back diodes on a flexible plastic substrate. The device exhibits current modulations with apparent saturation while applying various supply voltages to the base electrode. The operation mechanism could be attributed to the part of the induced current that flows through the base electrode rather than recombining at the base electrode. The effective mobility of the device is investigated by fitting the current–voltage characteristics at high voltages to the space-charge limited current (SCLC) model. Since the OBMT exhibits an operation behavior similar to that of conventional OTFTs, an inverter operated at low supply voltages can also be achieved by integrating a p-channel OBMT with a load resistor; such an inverter circuit and their voltage transfer curves are also demonstrated.

The schematic structure and a photograph of the OBMT are shown in Figure 1a and b, respectively. It consists of organic/metal/organic layers interposed between an anode and a cathode. In this device, all organic semiconductors, copper phthalocyanine (CuPc), pentacene, and *N,N′*-bis(naphthalen-1-yl)-*N,N′*- bis(phenyl)-benzidine (NPB), which are adopted as active materials, are conspicuously p-type in nature. The conduction in our device is hole-mediated, so that only highest occupied molecular orbital (HOMO) levels of the organic semiconductors are relevant to the device operation. The HOMO levels of NPB and pentacene are 5.8 and 5.0 eV below the vacuum level, respectively. The resultant energy barrier between base and emitter is 1.6 eV, and between base and collector is 0.8 eV. Since the collector-base barrier is lower than the emitter-base barrier by 0.8 eV, the holes with a higher energy are expected to pass through the thin metal base and to inject into the collector, while the thickness of the thin metal base is less than the mean free path in the base. The insertion of lithium fluoride (LiF) can further lower the aluminum (Al) Fermi level relative to the HOMO of NPB, resulting in an increase of the probability of the

[*] Dr. C.-W. Chu, Dr. D. Kekuda
Research Center for Applied Sciences
Academia Sinica
Taipei 115 (Taiwan)
E-mail: gchu@gate.sinica.edu.tw
Dr. C.-W. Chu
Department of Photonics
National Chiao Tung University
Hsinchu 300 (Taiwan)
S.-S. Cheng, Y.-C. Chuang, C.-W. Ou, Dr. M.-C. Wu
Institute of Electronics Engineering
National Tsing Hua University
Hsinchu 300 (Taiwan)

DOI: 10.1002/adma.200802506

WILEY InterScience DISCOVER SOMETHING GREAT
© 2009 WILEY-VCH Verlag GmbH & Co. KGaA, Weinheim

hole injecting into collector to form a higher constant current at a certain base voltage.[15,19] A thin Al grid, connecting two diodes as the base layer, was naturally formed on the rough organic surface and wired out by a fine Al stripe, and gold was used as the electrode for the upper and the lower diodes, respectively. Although there are energy barriers for each contact in this device, pentacene/Au and CuPc/Au have relatively smaller energy barriers, and can be regarded as Ohmic contacts. On the contrary, the NPB/LiF/Al for the EB diode and the Al/pentacene for the CB diode act as Schottky contacts.[20] Therefore, two diodes are connected back to back with the thin metal base electrode. The upper diode is described as emitter-base (EB) diode, and the lower diode as collector-base (CB) diode. The function of the CuPc layer is used to obtain a smooth Au surface morphology, which results in a lower leakage current in the CB diode. Using the above architecture, the current can be modulated from the emitter of EB diode to the CB diode instead of conducting through the base electrode while varying the base voltage.

The collector-to-emitter current (I_{CE}) versus collector-to-emitter voltage (V_{CE}) characteristics of the OBMT fabricated on the PET substrate at different base-to-emitter voltages (V_{BE}) are shown in Figure 2. The OBMT shows a high output current with an apparent saturation region at low voltages. The I_{CE} can reach up to $-9.33\,\mu A$ when both the V_{CE} and V_{BE} are applied at $-3\,V$. The on/off current ratio, which is defined as J_{CE} ($V_{BE} = -3\,V$)/J_{CE} ($V_{BE} = 0\,V$), is about 18 at $V_{CE} = -3\,V$. The off current can be reduced by optimizing the CuPc/pentacene thickness of the CB diode, and the on current can be enhanced by selecting the suitable work-function electrodes and also by reducing the thickness of the EB diode. These ways would further improve the device parameters, such as the on/off current ratio, and our current research is focused in that direction.

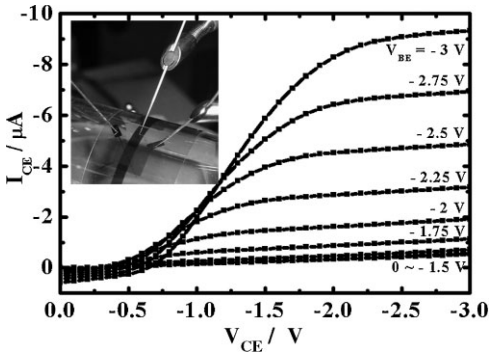

Figure 2. Collector-to-emitter current (I_{CE}) versus collector-to-emitter voltage (V_{CE}) in the base-to-emitter voltage (V_{BE}) range from 0 to $-3\,V$ at a step of $-0.25\,V$. The inset shows the picture of the OBMT fabricated on PET.

Although the devices exhibit typical p-channel characteristics similar to those of conventional OTFTs, they work under different scenarios. Since the thin Al grid, base layer, can effectively reduce the base recombination current, part of the emitter current would flow through the base electrode to form a collector current. Consequently, the I_{CE} can be modulated with apparent saturation by varying V_{BE}. This process would occur only when the thickness of the Al base electrode is less than the mean free path of the carriers. When the thin Al layer is replaced by a thicker Al film for the OBMT, resulting in a few places with the thickness smaller than the mean free path, the device shows lower current modulation without an apparent saturation region or no current modulation, which depends on the roughness of the organic surface and the thickness of Al base electrode.[21] As shown in Figure 2, the operation of an OBMT can be separated into two different regions, linear and saturation regions, depending on the voltages at the terminal. The clear modulation in I_{CE} occurs for the base voltages larger than 1.5 V. Hence, this voltage is presumed to be the threshold voltage of the device, which is slightly higher than the turn-on voltage of the emitter diode. The linear- and saturation-region mechanisms in our devices could be explained by taking into consideration the well-known Kirchhoff's law. As shown in Figure 1c, the potential drop at the collector–emitter junction is assumed to be a summation of the potential drop at the collector–base and the base–emitter junctions. This could be symbolized as: $V_{CE} = V_{CB} + V_{BE}$. According to this equation, it is inferred that, for a constant negative V_{BE}, V_{CE} is proportional to V_{CB}. When the CB diode is operated under forward bias and above its turn-on voltage, a positive current flows from the collector into the base. Moreover, the I_{CB} decreases when the V_{CE} becomes more negative. Because the I_{CE} is the summation of the constant tunneling current from the emitter and the collector-base current (I_{CB}), the collector current I_{CE} is proportional

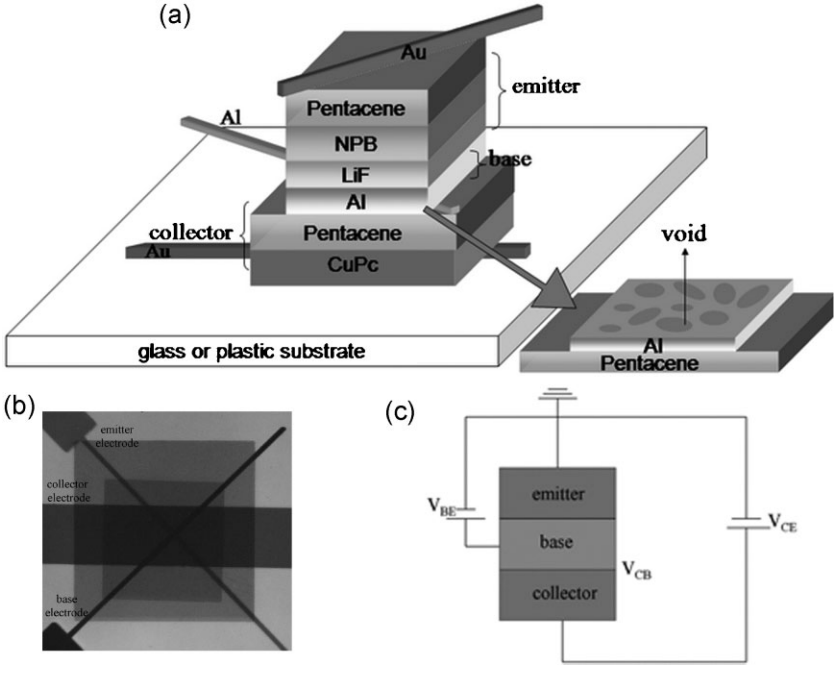

Figure 1. a) Schematic of the OBMT fabricated on a glass or plastic substrate. b) Photograph of the OBMT and c) measurement system for evaluating the device.

© 2009 WILEY-VCH Verlag GmbH & Co. KGaA, Weinheim

to the potential drop V_{CB}, and a positive current is observed when V_{CE} is near zero. Under those conditions, we denote the device as operating under the linear region. As the applied V_{CE} moves further towards large negative voltages, the forward bias becomes smaller and even turns into reverse bias on the CB diode. Since the I_{CB} becomes much smaller with respect to the constant tunneling current from the emitter, the saturation current is observed.

To investigate the transport properties of the vertical-type transistors, the carrier mobility in the active layer are studied. Because the OBMT is composed of two diodes, it is understood that the hole mobility in the emitter-base and collector-base diodes have happened at the same time and do not interact with each other. Therefore, the mean free time of the hole in the emitter-base diode is τ_{EB}, and the probability in the emitter-base diode is dt/τ_{EB}; correspondingly, dt/τ_{CB} is the probability in the collector-base diode. The effective hole mobility (μ^*) is given by:[22]

$$\frac{1}{\mu*} = \frac{1}{\mu_{EB}} + \frac{1}{\mu_{CB}} \tag{1}$$

where μ_{EB} is the hole mobility of the EB diode and μ_{CB} is the hole mobility of the CB diode. In order to calculate μ^*, μ_{EB} and μ_{CB} must be known. The current density (J) versus voltage (V) characteristics of the EB and CB diodes are shown in Figure 3. The applied voltage ($V_{applied}$) is corrected as the built-in potential (V_{bi}), which is equal to the difference in wok function between two contact electrodes of the diode. When the flat band condition is reached so that $V = V_{applied} - V_{bi}$, the current behaves quadratically as a function of voltage, which is common for low-mobility and disordered semiconductors.[23,24] It allows for a direct determination of the mobility through the SCLC model. Indeed, our J–V curves of the EB and CB diodes can be fitted well to the SCLC model, which shows as the Equation 1:

$$J = \frac{8}{9}\varepsilon_0\varepsilon_r\mu\frac{V^2}{L^3} \tag{2}$$

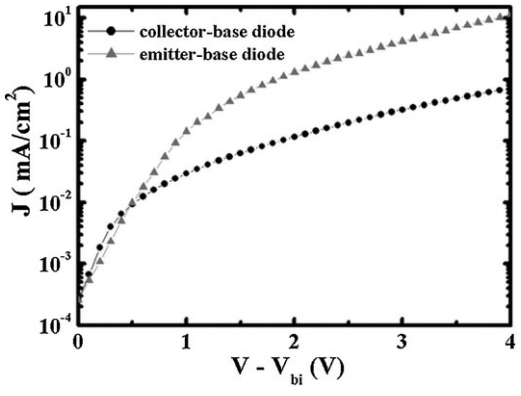

Figure 3. The square root of current density (J) versus voltage (V) characteristics of the CB and EB diodes. V_{bi} is defined as the wok function between two contact electrodes of the diode.

where J is the current density, ε_0 is vacuum permittivity, ε_r is the dielectric constant, V is voltage drop across the device, and L is the active-layer thickness. The hole mobility calculated from Equation 2 is 9.75×10^{-5} and $1.05 \times 10^{-5}\,cm^2\,V^{-1}\,s^{-1}$ for the EB and CB diodes, respectively. As a result of this, the extracted value of μ^* using Equation 1 is $9.48 \times 10^{-6}\,cm^2\,V^{-1}\,s^{-1}$. This value shows relatively large discrepancy as compared to the field-effect mobility of conventional OTFTs.[25] Although the OBMT has such a low mobility, the short channel length still allows it to be operated at relatively low voltages, and exhibits a high output current as compared to the conventional OTFTs.

The dynamic characteristics of the OBMT were measured by using a DC source, a function generator, and a digital oscilloscope. A sketch of the dynamic-response measurements of the OBMT is shown in Figure 4a. The V_B and an alternating signal with the rectangular wave were applied to base electrode, and the output signal was measured using a digital oscilloscope. The dynamic characteristics of OBMT at three different rectangular-wave frequencies of 100 Hz, 2 kHz, and 5 kHz are shown in Figure 4b–d. The output current density aligns the rectangular wave very well at 100 Hz, and suggests that the operated frequency can respond to the input frequency. When the input frequency is increased to a higher frequency of 5 kHz, as shown in the Figure 4d, the response waveform is distorted. Inspection of Figure 4c reveals that the half waveform can respond to the input frequency, and the applied frequency is determined, in this case, as the operation frequency of this device.

Having realized the OBMT operational procedures similar to those of conventional OTFTs, we have been able to fabricate inverters by connecting an OBMT with a resistor in series.[26] A sketch of the inverter with resistive load is shown in Figure 5a. The different resistors ranging from 100 to 500 kΩ at a step of 100 kΩ were connected with the collector of the OBMT at a supply voltage (V_{DD}) of −5 V. The voltage-transfer characteristics and their corresponding gains of the inverters are shown in Figure 5b. When the input voltage (V_{in}) is ''low voltage'', the device turns off and the output voltage (V_{out}) responds as ''high voltage''; on the contrary, when the input voltage is ''high voltage'', the device turns on and the output voltage becomes ''low voltage''. In the ideal case, the output voltage should be equal to V_{DD}, when the device is turned off. However, the device cannot be turned off completely, resulting in $|V_{out}|$ not being well-matched to $|V_{DD}|$. Therefore, we could not achieve a high voltage gain at this moment. As show in Figure 5b, the highest voltage gain was about 1.5, while the OBMT is connected to a 400 kΩ resistor and the voltage gain is changed by varying the resistor. The voltage gain can be further improved by lowering the off current of the device

In conclusion, we have demonstrated high-performance organic transistors based on a vertical structure. The OBMT can be fabricated on various substrates and measured in ambient conditions. The room-temperature processing of the components of the OBMT renders them feasible on flexible substrates. An inverter can be fabricated with the connection of an OBMT with suitable resistors. This is the first report on an inverter in a vertical-type transistor. Such an inverter represents a significant breakthrough, and could be applied to low-power and high-frequency electronic applications.

WILEY InterScience DISCOVER SOMETHING GREAT
© 2009 WILEY-VCH Verlag GmbH & Co. KGaA, Weinheim

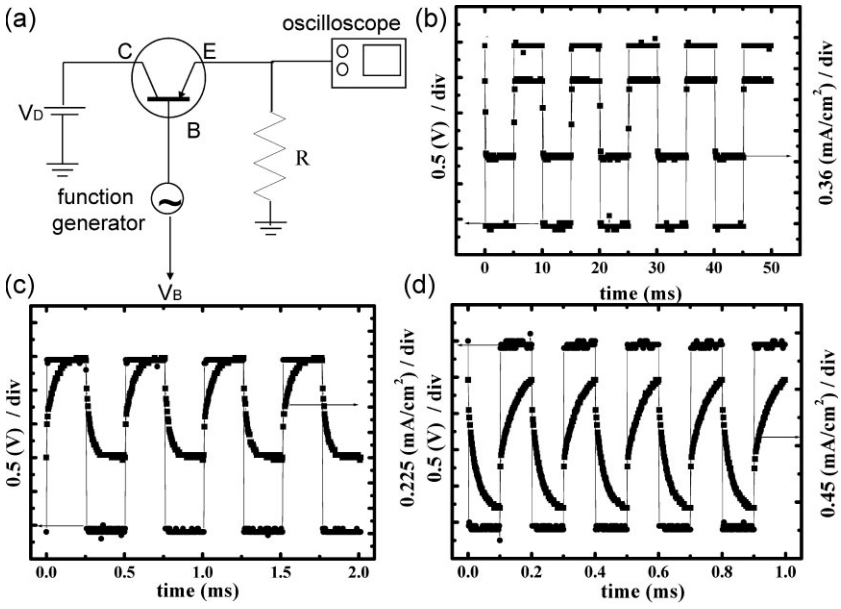

Figure 4. a) Sketch of the dynamic-response circuit for the OBMT. Input rectangular wave and output response waveform of b) 100 Hz, c) 2 kHz, and d) 5 kHz for the OBMT.

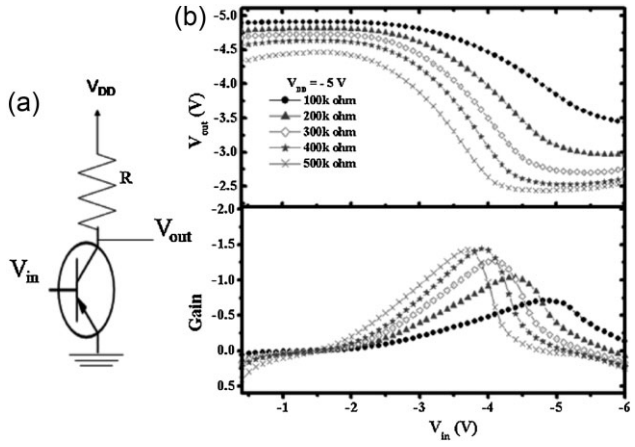

Figure 5. a) Schematic of an inverter comprising a vertical transistor with a load resistor. b) Measured transfer characteristics and corresponding gains of an inverter at $V_{DD} = -5$ V and different resistor ranges from 100 kΩ to 500 kΩ at 100 kΩ steps.

Experimental

The substrates were precleaned using detergent, acetone, isopropyl alcohol, and treated with an UV-ozone cleaner for 15 min. A Au layer 30 nm thick was deposited on the glass or PET substrate as the collector electrode. A CuPc layer (Luminescence Technology Corp.) 40 nm thick was thermally evaporated onto the Au layer to smoothen the surface morphology. A pentacene layer (Sigma–Aldrich, ≈98% purity) 280 nm thick was thermally evaporated as the collector layer at a rate of 0.10–0.13 nm s^{-1} from the crucible, and an Al layer 31 nm thick was thermally evaporated onto the pentacene layer as the base electrode. A thin Al layer of ≈10 nm was deposited as the base layer, and a LiF layer of 0.4 nm was thermally evaporated as the carrier-injection enhancement layer. Subsequently, a 20 nm thick NPB layer was thermally evaporated to enhance the carrier energy, and a pentacene layer 140 nm thick was thermally evaporated at the rate of 0.10–0.13 nm s^{-1} as the emitter layer. Finally, a Au layer 30 nm thick was thermally evaporated onto the pentacene layer as the emitter electrode. The above process was patterned by the metal mask. All organic materials and metal electrodes were deposited in a thermal-evaporation chamber at a base pressure of 10^{-6} Torr (1 Torr = 133.32 Pa). The active area of the device was 4.2×10^{-3} cm^2, which is defined as the intersection of emitter and collector electrodes. The current–voltage (*I*–*V*) characteristics of the devices were measured using a HP 4145B semiconductor parameter analyzer. The capacitance–voltage (*C*–*V*) measurements were performed using a HP 4980A Precision LCR meter. The operation frequency of the OBMT and conventional OTFTs were measured using a function generator Tektronix AFG 3022 and a signal oscilloscope Instek GDS-806S connected to a resistor of 300 kΩ. All the electrical characteristics of these devices were measured in the dark under ambient environment.

Acknowledgements

The authors are grateful to the National Science Council (NSC), Taiwan (95-2218-E-001-003), (96-2628-E-007-030-MY2), and Academia Sinica for financial support.

Received: August 27, 2008
Revised: December 18, 2008
Published online: March 4, 2009

[1] D. J. Monsma, J. C. Lodder, T. J. A. Popma, B. Dieny, *Phys. Rev. Lett.* **1995**, *74*, 5260.
[2] C. D. Sheraw, L. Zhou, J. R. Huang, D. J. Gundlach, T. N. Jackson, *Appl. Phys. Lett.* **2002**, *80*, 1088.
[3] C. J. Drury, C. M. J. Mutsaers, C. M. Hart, M. Matters, D. M. deLeeuw, *Appl. Phys. Lett.* **1998**, *73*, 108.
[4] F. Eder, H. Klauk, M. Halik, U. Zschieschang, G. Schmid, C. Dehm, *Appl. Phys. Lett.* **2004**, *84*, 2673.
[5] Y. Y. Lin, D. J. Gundlach, S. F. Nelson, T. N. Jackson, *IEEE Trans. Electron Devices* **1997**, *44*, 1325.
[6] A. Madan, M. P. Shaw, in *The Physics and Applications of Amorphous Semiconductor*, Academia, San Diego **1988**, p. 297.
[7] Y. Y. Lin, D. J. Gundlach, S. F. Nelson, T. N. Jackson, *IEEE Electron Device Lett.* **1997**, *18*, 606.
[8] H. Klauk, G. Schmid, W. Radlik, W. Weber, L. Zhou, D. C. Sheraw, J. A. Nichols, T. N. Jackson, *Solid-State Electron.* **2003**, *47*, 297.
[9] K. Kudo, M. Iizuka, S. Kuniyoshi, K. Tanaka, *Thin Solid Films* **2001**, *393*, 362.
[10] T. M. Ou, S. S. Cheng, C. Y. Huang, M. C. Wu, I. M. Chan, S. Y. Lin, Y. J. Chan, *Appl. Phys. Lett.* **2006**, *89*, 183508.
[11] M. S. Meruvia, I. A. Hummelgen, M. L. Sartorelli, A. A. Pasa, W. Schwarzacher, *Appl. Phys. Lett.* **2004**, *84*, 3978.
[12] K. I. Nakayama, S. Y. Fujimoto, M. Yokoyama, *Appl. Phys. Lett.* **2003**, *82*, 4584.

© 2009 WILEY-VCH Verlag GmbH & Co. KGaA, Weinheim

[13] Y. Yang, A. J. Heeger, *Nature* **1994**, *372*, 344.
[14] Y. C. Chao, M. H. Xie, M. Z. Dai, H. F. Meng, S. F. Horng, C. S. Hsu, *Appl. Phys. Lett.* **2008**, *92*, 093310.
[15] C. Y. Yang, T. M. Ou, S. S. Cheng, M. C. Wu, S. Y. Lin, I. M. Chan, Y. J. Chan, *Appl. Phys. Lett.* **2006**, *89*, 183511.
[16] L. P. Ma, Y. Yang, *Appl. Phys. Lett.* **2004**, *85*, 5084.
[17] S. H. Li, Z. Xu, L. P. Ma, Y. Yang, *Appl. Phys. Lett.* **2007**, *91*, 083507.
[18] K. Nakayama, S. Fujimoto, M. Yokoyama, *Appl. Phys. Lett.* **2006**, *88*, 153512.
[19] Y. C. Chao, S. L. Yang, H. F. Meng, S. F. Horng, *Appl. Phys. Lett.* **2005**, *87*, 253508.
[20] A. K. Mahapatro, S. Ghosh, *Appl. Phys. Lett.* **2002**, *80*, 4840.
[21] S. S. Cheng, C. Y. Yang, Y. C. Chuang, C. W. Ou, M. C. Wu, S. Y. Lin, Y. J. Chan, *Appl. Phys. Lett.* **2007**, *90*, 153509.
[22] A. D. Neamen, in *Semiconductor Physics and Devices: Basic Principles*, McGraw-Hill, Dubuque **2003**.
[23] C. Goh, R. Chiatzun, R. J. Kline, M. D. McGehee, E. N. Kadnikova, J. M. J. Fréchet, *Appl. Phys. Lett.* **2005**, *86*, 122110.
[24] C. Melzer, E. J. Koop, V. D. Mihailetchi, P. W. M. Blom, *Adv. Funct. Mater.* **2004**, *14*, 865.
[25] H. Klauk, U. Zschieschang, M. Halik, *J. Appl. Phys.* **2007**, *102*, 074514.
[26] K. H. Lee, J. M. Choi, S. Im, B. H. Lee, K. K. Im, M. M. Sung, S. Lee, *Appl. Phys. Lett.* **2007**, *91*, 123502.

WILEY InterScience® DISCOVER SOMETHING GREAT
© 2009 WILEY-VCH Verlag GmbH & Co. KGaA, Weinheim